Icarus 438 (2025) 116651

Contents lists available at ScienceDirect

Icarus

journal homepage: www.elsevier.com/locate/icarus

Spectral hydration features in nominally anhydrous minerals & implications for lunar remote sensing

Kierra A. Wilk [a,b,*], J.L. Bishop [c], A. Maturilli [d], C.M. Pieters [a], J.F. Mustard [a], K. Robertson [a]

[a] Brown University Providence, RI, United States of America
[b] NASA Goddard Space Flight Center Greenbelt, MD, United States of America
[c] SETI Institute Mountain View, CA, United States of America
[d] German Aerospace Center (DLR), Berlin, Germany

ARTICLE INFO

Keywords:
Moon
Infrared spectroscopy
Lunar regolith

ABSTRACT

The contributions of external and internal hydration (OH and H_2O) on the shape and strength of hydration related features at 3 and 6 μm for lunar relevant nominally anhydrous minerals were investigated under vacuum conditions. Understanding the effect of hydration on the reflectance spectra of lunar analog materials in the laboratory can provide insights into remote sensing observations of the lunar surface and the potential for 3 and/or 6 μm observations to determine the speciation of hydration on the Moon. We demonstrate changes in the shape and strength of the broad 3 μm absorption feature in olivine and anorthite that is associated with the removal of hydration under changing environmental conditions. The overlapping nature of OH and H_2O related absorption features in the ~3 μm region makes it difficult to uniquely determine the speciation of hydration. Despite evidence of H_2O loss in the 3 μm region, we do not observe the fundamental bending mode of H_2O at 6 μm, posing potential challenges for the detection H_2O on the lunar surface and throughout our solar system.

1. Introduction

Reflectance spectroscopy has played a prominent role in detecting hydration on the lunar surface. Water exhibits several absorption features in the near infrared spectral region, including the asymmetric and symmetric stretching vibrations of molecular water (H_2O) between 2.85 and 2.95 μm and the first bending overtone of the H_2O bending vibration at ~3.1 μm. Hydroxyl (OH) also exhibits its fundamental stretching vibration in this wavelength region, commonly between 2.7 and 2.9 μm, with the cationic environment and degree of hydrogen bonding heavily influencing the band position of this feature (Libowitzky, 2006). Three independent spacecraft - Chandryan-1 (Pieters et al., 2009), Deep Impact (Sunshine et al., 2009), and Cassini (Clark, 2009) - independently detected the widespread presence of a broad and asymmetric absorption feature near 3 μm, consistent with the presence of OH and/or H_2O on the lunar surface.

The lunar 3 μm "hydration" feature was initially identified in moderate and high latitude soils, with the relative strength of the 3 μm feature decreasing systematically with latitude and local time of day (Clark, 2009; Pieters et al., 2009; Sunshine et al., 2009). Several subsequent investigations have further acknowledged the correlation between the strength and distribution of the 3 μm hydration feature to instantaneous surface temperature and diurnal temperature variations (e.g., Chauhan et al., 2021; Grumpe et al., 2019; Honniball et al., 2020; Laferriere et al., 2022; S. Li and Milliken, 2017; McCord et al., 2011; Wöhler et al., 2017; Wohlfarth et al., 2023), suggesting that a portion of the observed hydration is surfical in nature and is influenced by local thermal conditions. The overlapping nature of H_2O and OH features in the 3 μm wavelength region, however, poses significant challenges in discerning the speciation and abundance of either species on the lunar surface. Neutron remote sensing from the Lunar Exploration Neutron Detector (e.g., Livengood et al., 2015) and ultraviolet spectroscopy from the Lyman Alpha Mapping Project (e.g., Hendrix et al., 2019) onboard the Lunar Reconnaissance Orbiter further support diurnal variations in lunar hydration, though are unable to distinguish OH and H_2O.

Fortunately, in addition to the H_2O/OH absorption features in the 3 μm region, molecular H_2O exhibits its fundamental bending mode at ~6 μm, where there are no overlapping OH vibrations, potentially circumventing the ambiguity and need to distinguish between H_2O and OH features. Stratigraphic Observatory for Infrared Astronomy (SOFIA) telescopic observations have inferred the existence of H_2O on the lunar surface via the presence of a weak emission feature at ~6 μm (Honniball

* Corresponding author at: Brown University Providence, RI, United States of America.
E-mail address: kierra_wilk@brown.edu (K.A. Wilk).

https://doi.org/10.1016/j.icarus.2025.116651
Received 24 December 2024; Received in revised form 6 May 2025; Accepted 11 May 2025
Available online 12 May 2025

et al., 2021, 2022; Reach et al., 2023). As such, repeated and coordinated 3 and 6 μm observations has the potential to resolve the speciation of hydration on the lunar surface and capture the migration of this volatile across the surface.

Wilk et al., 2024 assessed spectral variations at 3 and 6 μm due to the thermal removal of surface adsorbed H_2O under dry air conditions for nominally anhydrous minerals (including olivine, pyroxene, and plagioclase) and mature lunar soils. Clear and systematic changes in the strength and shape of the 3 μm feature associated with the removal of H_2O were well documented. No distinguishable features, however, could be attributed to the presence or removal of H_2O at 6 μm, calling into question the possibility of observing diurnal variations in H_2O content on the lunar surface. Additional laboratory work is needed to understand the effect of a vacuum environment on hydration related features at 3 and 6 μm.

In addition to any surficial hydration on the lunar surface, Li and Milliken, 2017 and Milliken and Li, 2017 have suggested that hydration encapsulated within volcanic, agglutinitic, and impact glasses likely contributes to the observed 3 μm hydration feature and would remain unaffected by diurnal temperature variations. In situ analysis of returned lunar samples have measured detectable amounts of water in mare basalt melt inclusions (e.g., Hauri et al., 2011; Hu et al., 2021; Stephant et al., 2020), pyroclastics (e.g., Saal et al., 2008, 2013), and apatite (e.g., Barrett et al., 2023; Boyce et al., 2010), further suggesting that interior water contents likely contribute to the strength of hydration related features in both remote sensing and laboratory spectra.

In this work, we build on the work of Wilk et al., 2024 to continue exploring the nature of hydration related features in the 3 and 6 μm region for two lunar relevant nominally anhydrous minerals, olivine and anorthite. Here we assess the effect of a vacuum environment on hydration related features at ambient temperatures. The samples were further thermally processed to evaluate internal hydration contributions to the strength and shape of hydration related features. Investigating the effects of internal and external hydration on the reflectance spectra of lunar relevant minerals can offer valuable insights into what may be observed on the lunar surface and the feasibility in which 3 and/or 6 μm observations may be able to address the speciation of hydration on the Moon.

2. Methods

2.1. Experimental procedure

Several grams (~3–4 g) of relatively pure terrestrial olivine (San Carlos, Mg#90) and anorthite (Miyake-Jima; An>90) were dry sieved to <45 μm particle size separates. Bi-directional and hemispherical reflectance measurements (1–25 μm) of the unaltered samples were acquired using a Bruker Fourier Transform IR (FTIR) spectrometer under vacuum conditions (10^{-3} Torr) in the Planetary Spectroscopy Laboratory at the German Aerospace Center (DLR) in Berlin. Reflectance measurements were first acquired under vacuum conditions once the vacuum system reached its target pressure (10^{-3} Torr), followed by two more measurements at 15 min intervals to demonstrate measurement consistency and that the vacuum system was stabilized. Following these measurements, the samples were later prepared in a steel sample dish (depth = 1.5 mm) and gradually heated under a ~ 10^{-3} Torr vacuum for approximately 9 h, with the olivine and anorthite sample dish reaching a maximum temperature of 873 K and 887 K respectively. This heating processes was employed as a mechanism to dehydrate the samples and to evaluate irreversible changes in hydration content (i.e., internal water).

After heating, the samples were removed from vacuum and subsequently cooled in a desiccator at ambient pressures overnight. Bi-directional and hemispherical reflectance measurements of the dehydrated samples were acquired under vacuum conditions the following day, again including an initial measurement once the sample chamber reached is target pressure and twice more at 15 min intervals. These measurements were obtained at a spectral resolution of 4 cm^{-1} using a MCT detector, with 500 and 1000 scans per measurement for the bi-directional and hemispherical measurements respectively. Reflectance measurements were made relative to a diffuse gold standard positioned in vacuum conditions for 10 min before the reference measurement was taken. Additional measurements (0.3–99 μm) of the samples under purged gas conditions were acquired using a Nicolet NEXUS 870 FTIR in the NASA Reflectance Experiment LABoratory (RELAB) at Brown University, with a 4 cm^{-1} resolution relative to a diffuse gold standard in purged dry air gas conditions. This interlaboratory comparison allowed us to assess the reliability of our results and to more readily compare our spectra to the extensive catalog of samples, including lunar soils, that have also been measured at RELAB under identical conditions.

2.2. XRD

X-ray diffraction (XRD) measurements were acquired on a subset of the sample prior to and after heating to evaluate the purity of the original endmember samples and to assess any possible changes to the crystal structure in the heated samples. Samples were analyzed with a Bruker D2 Phaser XRD equipped with a Cu Kα X-ray source, a 0.6 mm divergence slit, 0.3 mm anti-scatter shield, 2° soller slits, a Ni filter, and a LYNXEYE detector. Each sample was measured from 10°-90° 2θ with a 0.02° 2θ step size and a 6 s/step dwell time. The resultant diffraction patterns were evaluated with the Bruker DIFFRAC.EVA software package in tandem with the International Centre for Diffraction Data (ICDD) PDF-2 crystallographic database and mineral abundances were determined via Rietveld refinement (see supplemental text). XRD data of the pre- and post-heated samples are provided in **Supplementary Fig. 1**.

2.3. Spectral parameters

To evaluate differences between samples in the shapes and slopes of spectral features in the 3 μm region, we first normalized the spectra at 2.4 μm. We then calculated several spectral parameters to characterize the strength and shape of the 3 μm hydration feature, including the 3 μm band minimum position, band depth (BD), integrated band depth (IBD), and full width half maximum (FWHM). Each spectrum was divided by its continuum (defined between 2.4 and 4.0 μm for the ~3 μm band) to produce a continuum removed spectrum. The band depth is defined as 1 minus the continuum removed reflectance at a given wavelength (λ). Both the olivine and anorthite sample had ~3.4 and ~ 3.5 μm C—H absorptions we attribute to minor hydrocarbon organic contamination. Given this, when calculating the FWHM and IBD (eq. 1), reflectance values for the wavelength channels between 3.35 and 3.55 μm were removed and linearly interpolated over this wavelength regime. The FWHM is defined by the width (measured in μm) of the absorption at half of the maximum strength of the feature. The IBD is normalized by the integrated maximum band depth (BD_{MBD}), where the normalized depth has a maximum possible band depth (MBD) value of 1 for each measured wavelength and λ_{min} is 2.4 μm and λ_{max} is 4 μm.

$$IBD = \frac{\int_{\lambda_{min}}^{\lambda_{max}} BD(\lambda) \bullet d\lambda}{\int_{\lambda_{min}}^{\lambda_{max}} BD_{MBD}(\lambda) \bullet d\lambda} \quad (1)$$

Additionally, we converted our reflectance spectra to single scattering albedo to estimate water (OH/H2O) content in the 3 μm region using the Effective Single-Particle Absorption Thickness (ESPAT) function. The single scattering albedo represents the interaction of a photon with a single particle and Hapke, 2012 demonstrated the reflectance spectrum, R, can be related to single scattering albedo (w) by

$$R(i,e,g) = \frac{w}{4(\cos(i)+\cos(e))} \bullet \{[1+B(g)]p(g)+H(\cos(i))H(\cos(e))-1\} \quad (2)$$

where *i, e,* and *g* are the incidence, emergence, and phase angle respectively. For the spectral measurements acquired at the DLR, the viewing geometry is $i = 30°$, $e = 0°$, and $g = 30°$ and for the RELAB measurements the viewing geometry is $i = 30°$, $e = 30°$, and $g = 60°$. We follow the parameterization of the Hapke model demonstrated in S. Li and Li, 2011, where the backscattering function, *B(g)*, is approximated to be

$$B(g) = \left(1 + \left(\frac{1}{h}\right)\tan\left(\frac{g}{2}\right)\right)^{-1} \quad (3)$$

and the angular width parameter of the opposition effect, *h*, is $h = -3/8\ln(1-\phi)$. We set the filling factor, ϕ, to be consistent with the lunar regolith ($\phi = 0.41$) (Bowell et al., 1998). The H function, *H*, is approximated by

$$H(x,w) = \left\{1 - (1-\gamma) \bullet x \bullet \left[r_0 + (1 - 0.5r_0 - r_0 x) \bullet \ln\left(\frac{1+x}{x}\right]\right]\right\}^{-1} \quad (4)$$

where *x* is either the cosine of the incidence or emergence angle, $\gamma = \sqrt{1-w}$, and $r_0 = \frac{(1-\gamma)}{(1+\gamma)}$. Finally, the phase function, P(g), is

$$P(g) = 1 + b\cos(g) + c\left(1.5\cos^2(g) - 0.5\right) \quad (5)$$

where the forward scattering of the minerals, b and c, are set to −0.4 and 0.25 respectively (Mustard and Pieters, 1989). Eq. [2] can then be solved for *w* at each wavelength using the observed reflectance values.

Due to differences in absolute reflectance between the spectra measured at RELAB and at the DLR, we scale the DLR bi-directional reflectance spectra to the RELAB spectra at 2 μm where there are no mineral or water related absorptions. The reflectance spectra are then converted to single scattering albedo, and we remove the continuum between 2.4 and 4.0 μm in the 3 μm region to account for any differences in spectral slopes between the samples. The ESPAT parameter [Eq. 6] is linearly proportional to water content and the empirical relationship between total water content and the ESPAT parameter at ~2.9 μm has been described as the weight percent water = $4.9130 \cdot \text{ESPAT}_{\sim 2.9\mu m}$ (Milliken and Mustard, 2005).

$$ESPAT(\lambda) = \frac{1 - w(\lambda)}{w(\lambda)} \quad (6)$$

To evaluate changes in the 6 μm region, we normalized the reflectance spectra to unity at 5.7 μm and provide spectral ratios of the unheated olivine and anorthite sample to the most dehydrated sample (i.e., bottom olivine and mixed anorthite).

3. Results

Following the heating of the olivine and anorthite samples to 873 K and 887 K respectively, the samples cooled down in a desiccator at ambient temperatures and pressures overnight and were subsequently distributed into new sample dishes. During the dehydration process, the olivine sample at the bottom of the dish oxidized, indicated by its red in colour appearance. The olivine sample was then partitioned into 3 separates: sample from the top of the dish, sample from the bottom of the dish, and a mixed sample from the dish. The anorthite sample did not experience a similar oxidation reaction and was consequently only partitioned as a mixed sample from the dish. The nomenclature of a top sample, mixed sample, and bottom sample is used going forward and this order can generally be thought of as the samples becoming progressively more dehydrated, as the bottom sample had more direct contact with the heated sample dish. XRD of the olivine sample from the bottom of the dish indicates the formation of ~1 wt% hematite (Supplementary Fig. 1), which is not observed in the unheated olivine sample, and the abundance of any hematite in the mixed and top olivine sample is likely <1 wt%.

Reflectance spectra [0.3–8 μm] of the olivine and anorthite samples measured in RELAB under dry purged air conditions are shown in Fig. 1 and the RELAB specimen identifiers are provided in **Supplementary Table 1**. We note that the heated olivine samples measured in RELAB exhibit stronger organic features at 3.4 and 3.5 μm than observed in the bi-directional and hemispherical spectra measured at DLR. This is most likely attributed to increased organic contamination during sample handling. The RELAB reflectance spectra, which were acquired under purged dry air conditions, otherwise exhibit the same sample absorption features and relative changes as the reflectance spectra measured under vacuum conditions. As such, we discuss only the bi-directional spectra (Fig. 2) in further detail below and provide additional hemispherical spectra in **Supplementary Figs. 2–4**.

3.1. The 3 μm region

All the samples exhibit a broad absorption feature in the 3 μm region (Fig. 3). When measured at ambient conditions, the samples display sharp atmospheric components shortward of 2.83 μm and all samples contain minor organic contaminants that contribute three narrow spectral bands at ~3.37, 3.42, and 3.51 μm, characteristic of aliphatic CH stretching vibrations (e.g., Bishop et al., 1998). These features were carefully avoided, as described in section 2.3 during the data analysis to avoid interference with the interpretation of the much stronger hydration related features. In Fig. 4 we present the IBD, band minimum position, and FWHM parameters of the 3 μm absorption for each of our samples, in addition to the total water content derived from the ESPAT parameter. Total water contents derived from the RELAB spectra can be found in **Supplementary Fig. 5.**

At ambient conditions, both olivine and anorthite have a broad 3 μm feature with their band minima centered at ~2.9 μm and an estimated water content of 320 and 409 ppm respectively. Exposure to a vacuum environment for 30 min decreased the olivine sample's water content by 160 ppm and the anorthite sample's water content by 209 ppm, with a notable 35 % and 30 % decrease in the IBD for each sample. The relative appearance of the 3 μm feature remains unchanged, with negligible differences in the FWHM value between the ambient and vacuum environment measurements.

The dehydration process removed considerable amounts of hydration from the samples. The bottom olivine sample exhibited a 90 % decrease in IBD resulting in a derived total water content of 21 ppm while the mixed anorthite sample experienced a 66 % decrease in IBD and a derived total water content of 57 ppm. Olivine's 3 μm feature became considerably narrower with progressive dehydration and its band minimum remained near ~2.91 μm (though it visually appears to shift towards short wavelengths due to the bottom of the absorption feature being relatively flat). In addition to the band minimum within the broad 3 μm feature, there is a clear additional inflection at 3.1 μm for

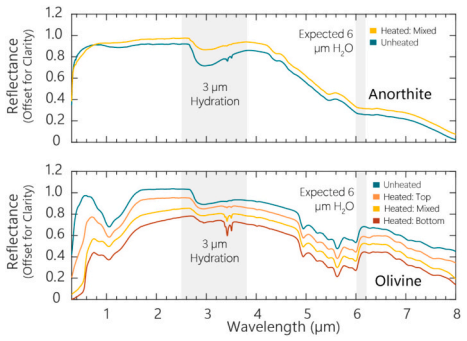

Fig. 1. RELAB reflectance spectra (0.3–8 μm) of olivine and anorthite before and after heating to 873 K and 887 K, respectively. RELAB specimen identifiers can be found in **Supplementary Table 1**.

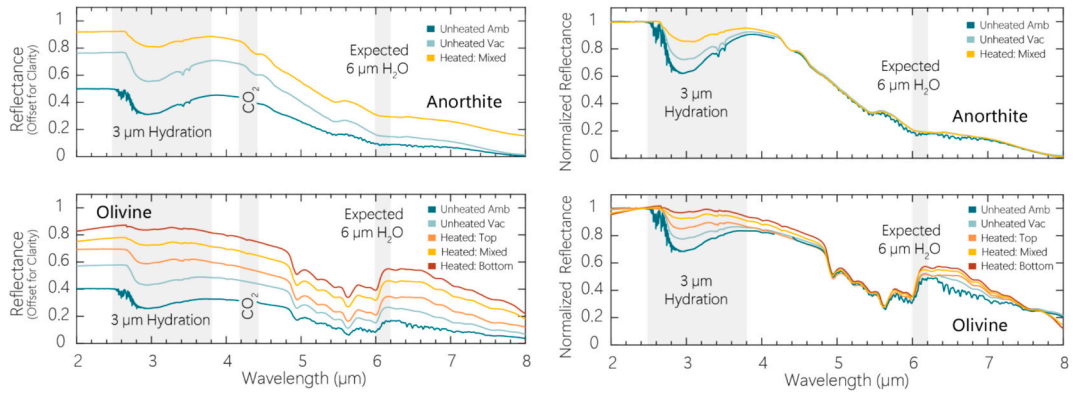

Fig. 2. DLR bi-directional reflectance spectra (2–8 μm) on the left and reflectance spectra normalized to unity at 2.4 μm on the right, of anorthite and olivine acquired under ambient and vacuum (~10^{-3} Torr) conditions before and after heating to 873 K and 887 K respectively. For the unheated ambient spectra, wavelengths between 4.1 and 4.4 μm were removed due to large atmospheric CO_2 absorptions. All the heat-treated samples were measured under vacuum conditions at room temperature.

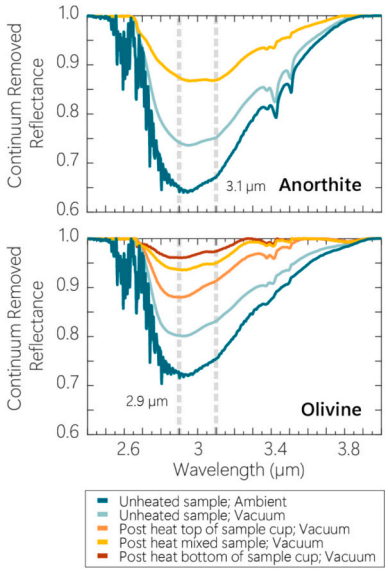

Fig. 3. Continuum removed bi-directional reflectance spectra of anorthite and olivine acquired under ambient and vacuum (~10^{-3} Torr) conditions before and after they have been heated to 873 K and 887 K respectively. Both olivine and anorthite exhibit absorption features near ~2.9 and ~ 3.1 μm (represented by a gray dashed line).

the unheated vacuum, top, mixed, and bottom olivine sample's spectra. Anorthite's 3 μm feature was centered at ~2.94 μm and remained broad following dehydration. The band minimum shifted towards slightly longer wavelengths, with a clear inflection in the 3 μm feature at 3.1 μm in addition to the band minimum at ~2.94 μm.

3.2. *The 6 μm region*

In the intermediate infrared (IMIR; 4–8 μm) region, H_2O exhibits its fundamental bending mode between 6.0 and 6.2 μm (Nyquist et al., 1997) and silicate minerals also have several absorption features in this wavelength region (e.g., Lane and Bishop, 2019; Salisbury et al., 1987). Combinations and overtones of fundamental silicate vibrations in the mid infrared (MIR; 8–15 μm) create a plethora of absorption features in the IMIR region. Most notably, olivine has two prominent absorption features at 5.6 and 6.0 μm whose band minimum position shift systematically with Mg content (Kremer et al., 2020). Additionally, anorthite exhibits a weak absorption feature at ~5.4 μm and a broad flat-bottom absorption feature near ~6.2 μm. We provide a zoomed in normalized view of the 6 μm region and ratioed spectra of the olivine and anorthite samples in Fig. 5 and Fig. 6 to evaluate the role of H_2O in this wavelength region.

Contributions from atmospheric water vapor occur between 5 and 7.5 μm in the ambient sample measurements, making it difficult to assess the presence of surface adsorbed water in the 6 μm region and consequently differences in surface hydration between ambient and vacuum conditions. We do, however, observe no difference or change in reflectance between the three vacuum measurements at 6 μm for both the olivine and anorthite samples (Fig. 5A,C). Dehydration of olivine exhibited no discrete features or changes in reflectance that could be

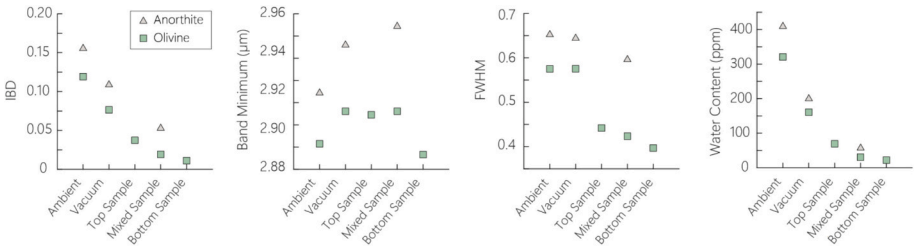

Fig. 4. Spectral parameters of the 3 μm absorption feature, including the integrated band depth (IBD), band minimum position, and full width half maximum (FWHM) were calculated using the 3 μm continuum removed reflectance spectra. Water content is estimated using the ESPAT parameter from single scattering albedo. The unheated olivine sample measured under ambient conditions has an estimated water content of 320 ppm and 160 ppm when measured under vacuum conditions. The top, mixed, and bottom olivine sample have 69 ppm, 30 ppm, and 21 ppm water contents respectively. The unheated anorthite sample measured under ambient and vacuum conditions is 409 ppm and 200 pm, with the mixed sample having an estimated 51 ppm water content. Green squares represent olivine and gray triangles represent anorthite. (For interpretation of the references to colour in this figure legend, the reader is referred to the web version of this article.)

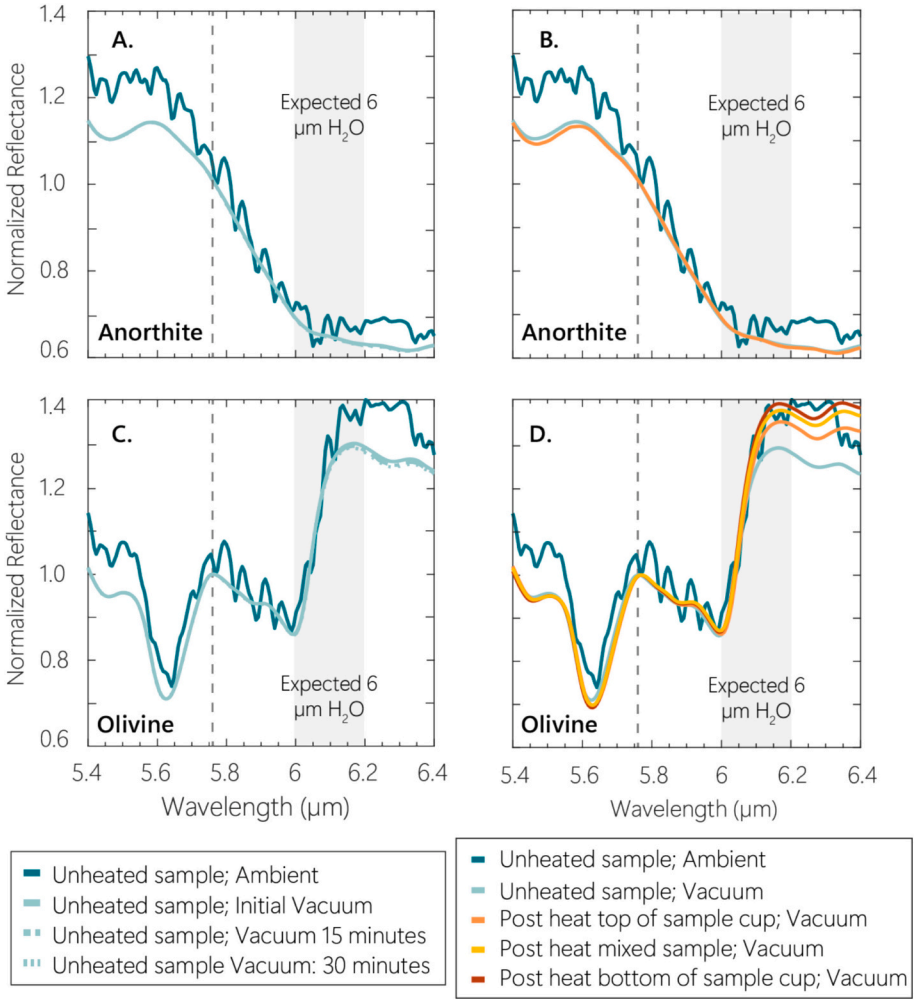

Fig. 5. Bi-directional reflectance spectra (5.4–6.4 μm) of olivine and anorthite, normalized to unity at 5.7 μm indicated by the gray dashed line. The expected band position of the 6 μm H_2O absorption is shaded in gray. Differences in reflectance spectra between the ambient measurement and the sample under vacuum conditions for 0, 15, and 30 min are shown in A and C. Reflectance spectra of the sample pre- and post-heating are shown in panels B and D.

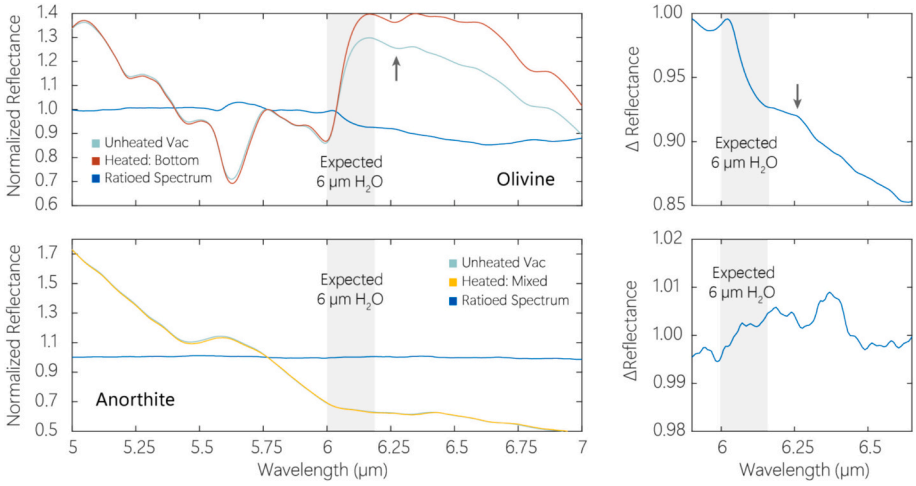

Fig. 6. Normalized bi-directional reflectance spectra (5–7 μm) of olivine and anorthite normalized to unity at 5.7 μm and a ratioed spectrum of the unheated sample to the most heated sample. The expected band position of the 6 μm H_2O absorption is shaded in gray. A zoomed in view of the ratioed reflectance spectrum is shown on the right. Neither olivine nor anorthite exhibit a water related feature at 6 μm in the ratioed spectra. The gray arrow in the olivine plot indicates the location of the 6.26 μm absorption feature that increases in strength with progressive dehydration.

attributed to the presence and/or removal of water in the 6 μm region (Fig. 5D). The top, mixed, and bottom heated olivine samples exhibit a flatter spectral slope between 6.1 and 6.6 μm compared to the unheated olivine sample which has a much steeper spectral slope in this wavelength region. In addition to the 5.6 and 6.0 μm features, all the olivine samples exhibit an absorption feature with a band minimum centered near 6.26 μm that increases in strength with progressive dehydration (Fig. 7). In the ratioed spectrum, the removal of H_2O in the 6 μm region should manifest as a negative feature. While the changes in spectral slope, as well as the strengthening of the 6.26 μm absorption feature is evident in the ratioed olivine spectrum, we do not observe any negative features that can be associated with the removal of H_2O between the unheated and bottom olivine sample (Fig. 6). Dehydration of the anorthite sample resulted in no observable changes in reflectance between the unheated and mixed anorthite sample under vacuum conditions in the 6 μm region (Fig. 5B). The ratioed anorthite spectrum provides no further evidence of water removal, with 0.006 % maximum variation between the unheated and mixed anorthite sample in the 6 μm region.

4. Discussion

4.1. State of hydration

Nominally anhydrous minerals, including olivine and anorthite, have a variety of mechanisms in which they can incorporate OH/H_2O. Externally, monolayers of water molecules may exist on mineral surfaces via chemisorption, in which H_2O covalently bonds at electropositive surface sites causing the dissociation of H_2O and the formation of OH groups or through the hydrogen bonding of H_2O to other H_2O and OH molecules (Dyar et al., 2010; Hibbitts et al., 2011). Chemisorbed OH is more thermally stable than chemisorbed H_2O, with H_2O desorption typically occurring between 180 and 400 K and terminally bonded OH desorption occurring between 500 and 600 K (Dyar et al., 2010; Hibbitts et al., 2011). We measured our samples under vacuum (10^{-3} Torr) to remove loosely bound hydration, with the predominant species removed likely being H_2O given that OH is more strongly bound and consequently more stable than H_2O. Despite the presence of a vacuum environment surface hydration likely persists, as small amounts of hydration can exist stably on the surface of minerals even under ultra-high vacuum ($<10^{-8}$ Torr) (Hibbitts et al., 2011).The effect of removing the loosely held surficial component is discussed in further detail in Section 4.2.

Water can also be incorporated into olivine and anorthite internally in the form of H_2O within fluid inclusions and OH as structural defects. We gradually heated our samples to upwards of ~870 K to remove interior hydration components and assess their contribution to the observed hydration features. Changes in the strength and shape of the 3 μm feature in consequence of the heating are both permanent and non-reversible, indicating that interior hydration was lost albeit not completely removed due to the 3 μm feature remaining even in our most heated samples. The effect of removing interior hydration is discussed in further detail in Section 4.2.

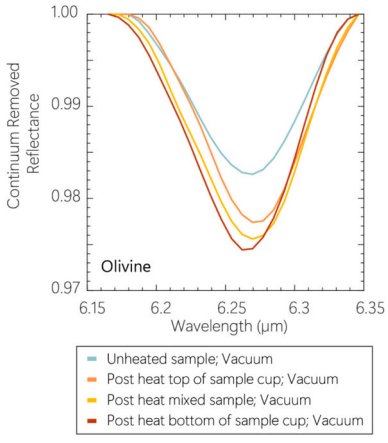

Fig. 7. Continuum removed reflectance spectrum (6.15–6.35 μm) of olivine's 6.2 μm absorption feature. The strength of the feature increases with progressive dehydration and oxidation of the sample.

4.2. Variability in the 3 μm Region

At ambient pressures and temperatures, external hydration exists on the surface of the olivine and anorthite samples, influencing the strength and shape of the 3 μm feature. The introduction of the olivine and anorthite samples to a vacuum environment decreases the strength of the 3 μm feature and is consistent with the loss of surface adsorbed H_2O, rather than surficial OH. Approximately 160 ppm and 209 ppm of water was removed from the olivine and anorthite samples, respectively, via exposure to a vacuum environment. While the removal of surface adsorbed H_2O via vacuum decreases the 3 μm band strength, we observe little change in the FWHM of the 3 μm feature of either sample and see only minor shifts in the band minimum position (Figs. 3,4). Wilk et al., 2024 performed low temperature heating experiments under ambient pressures to remove surface adsorbed H_2O and noted much greater variability in the strength and shape of the 3 μm feature than what is observed here. Most notably, they found olivine's 3 μm feature became considerably narrower, with a band minimum that shifted towards lower wavelengths with surficial H_2O loss. The difference in 3 μm behavior between these two studies is likely due to the degree in which H_2O has been removed from the mineral surfaces, where the thermal removal of H_2O performed in Wilk et al., 2024 was a more efficient mechanism to remove surficial H_2O, resulting in greater spectral variability. We postulate we would observe similar changes in band shape and minimum position with the introduction of low temperature heating to remove additional hydration from the surface. Future investigations performing low temperature heating under vacuum conditions, while collecting in-situ reflectance measurements, would be valuable to understand fully how temperature and vacuum work in tandem to influence the behavior of the 3 μm hydration feature for a variety of mineral compositions.

While it is probable that small amounts of hydration persist on the surfaces of the olivine and anorthite grains, the incomplete removal of the 3 μm feature in vacuum further suggests that internal hydration, in the form of structural OH and potentially H_2O in fluid inclusions, contributes to the observed 3 μm feature. Indeed, the progressive removal of internal hydration in the 3 μm region can be observed in the top, mixed, and bottom olivine and anorthite samples (Fig. 3). Structural defects in olivine provide a mechanism for hydrogen bearing species, such as OH, to be incorporated into olivine's crystal lattice and there have been numerous studies that have correlated specific defects to OH absorption features in the infrared (see Le Losq et al., 2019; Y. (Will) Li et al., 2022 and references therein). Hydroxyl associated with silicon vacancies may produce absorption features between 2.75 and 2.85 μm, OH associated with trivalent cations in Mg vacancies may produce absorptions between 2.94 and 3.0 μm, and OH associated with metal (Mg^{2+} or Fe^{2+}) vacancies may produce absorption features near ~3.1 μm. Our olivine samples' 3 μm feature (Fig. 3) is centered near 2.91 μm, with an additional absorption feature near 3.1 μm, which may be attributed to OH associated with trivalent cations in Mg vacancies and metal vacancies respectively. It is important to note, however, that H_2O gives rise to the asymmetric and symmetric stretching vibrations of the water molecule between 2.85 and 2.95 μm as well as the first bending vibration overtone of H_2O near 3.1 μm. Olivine can host small amounts of H_2O in fluid inclusions and the presence of water cannot be excluded, as both the band minimum and 3.1 μm absorption are also consistent with H_2O. Fig. 8 highlights the overlapping nature of H_2O and OH related absorptions in olivine and anorthite, illustrating that the presence of an absorption or band minimum may not reliably indicate speciation in the

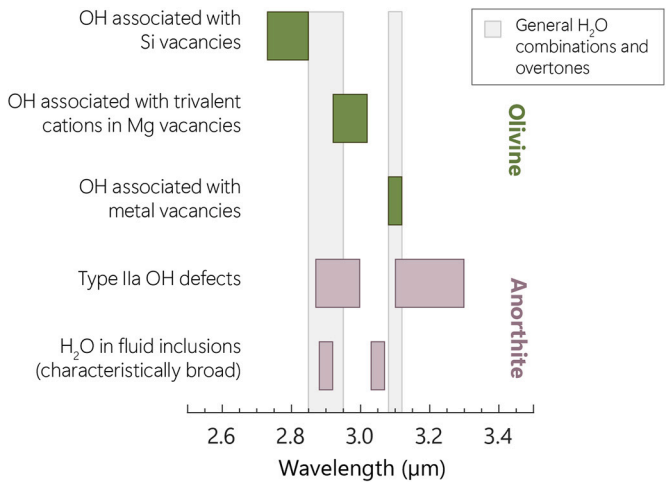

Fig. 8. The expected band positions of OH and H_2O related features in olivine (green) and anorthite (pink). While the ability of olivine to host H_2O in fluid inclusions is noted in the literature, there were no specific band assignments for H_2O fluid inclusions as there were for anorthite. As such, we also note the expected band positions of general H_2O combinations and overtones in gray. Many of the expected band positions in the 3 μm region overlap, making it difficult to uniquely determine the speciation of hydration. Band assignments of OH and H_2O in olivine and anorthite are from Le Losq et al., 2019, Y. (Will) Li et al., 2022 and Johnson and Rossman, 2004. (For interpretation of the references to colour in this figure legend, the reader is referred to the web version of this article.)

3 μm region. Irrespective of the speciation, the bottom olivine sample lost ~140 ppm of water during the dehydration process and the progressive removal of interior hydration is evident in the top, mixed, and bottom olivine sample via the permanent weakening and narrowing of the 3 μm feature.

Anorthite, the calcium endmember of the plagioclase feldspar series, can structurally incorporate small amounts of OH and non-structurally incorporate small amounts H_2O into its aluminosilicate network, and the assignment of hydrous species in the infrared spectra of feldspars has been reviewed in depth by Johnson and Rossman, 2004. Type IIa OH defects in feldspars, which are commonly found in plagioclase, are characterized by their broad absorption bands centered near 2.89–2.98 μm and 3.12–3.28 μm. Fluid and melt inclusions are non-structural mechanisms in which H_2O may be incorporated into plagioclase. Absorption features due to fluid inclusions are characteristically broad, with absorption minimums occurring near 2.9 μm and shoulder features near 3.05 μm, with melt inclusions giving rise to asymmetric absorptions centered near 2.8 μm. Anorthite's broad 3 μm feature (Fig. 3) whose band minimum is centered at 2.94 μm with an additional absorption feature at 3.1 μm is consistent with both type IIa OH defects and H_2O in fluid inclusions. Given the overlapping nature of OH and H_2O features, the exact speciation of the interior hydration component cannot be uniquely determined in the 3 μm region though an estimated ~143 ppm of water was permanently removed during the heating process.

4.3. The 6 μm region

4.3.1. Fundamental bending mode of H_2O

The fundamental bending vibration of water gives rise to an absorption feature between 6.00 and 6.2 μm (Nyquist et al., 1997) and can be used to distinguish the presence of H_2O from OH. We analyzed our reflectance spectra for absorption features and changes in reflectance we could attribute to the presence and/or removal of H_2O. We estimate ~320 ppm of water is present in the olivine sample and ~ 400 pm of water is present in the anorthite sample when measured under ambient conditions. While we interpret the changes in the strength of the 3 μm feature with vacuum exposure to be consistent with the removal of surface adsorbed H_2O, in addition to internal H_2O in fluid inclusions being perhaps partially responsible for the observed 3 μm character, we do not observe the fundamental bending absorption in the 6 μm region.

We present three possible explanations as to why the 6 μm feature is not discernible in these samples:

1. Water is not present and OH is the only hydrous species responsible for the 3 μm feature.
2. Silicate related absorption features in this region suppress the detection of H_2O.
3. The amount of H_2O present is not sufficient to produce a 6 μm feature.

We find explanation 1 to be the most unlikely scenario, as we postulate the exposure to the vacuum environment primarily removed surficial H_2O rather than OH. The inability to resolve surface adsorbed H_2O on nominally anhydrous minerals in the 6 μm region is consistent with Wilk et al., 2024, where surface hydration was thermally removed in temperature regimes expected for H_2O desorption, not OH, yet the 6 μm feature remained undetected. We do note, however, that while the 2.9 and 3.1 μm absorption features in olivine and anorthite are consistent with both internal OH and H_2O, we have no independent mechanism to determine the speciation of the hydration in either sample. It is possible that only OH is incorporated internally and largely contributes to the 3 μm feature, though this cannot explain why we do not observe the surfical H_2O components in the 6 μm region. It has been previously noted that strong absorptions due to the aluminosilicate network of feldspars can prevent the detection of the fundamental H_2O absorption at 6 μm (Johnson and Rossman, 2004). Olivine also exhibits strong silicate related absorption features in the 6 μm region (Kremer et al., 2020) and it would not be unreasonable to expect that the presence of these features could stifle the detection of H_2O as well. Finally, differences in the absorption coefficient values of H_2O at 3 and 6 μm may be responsible for the lack of an observable 6 μm feature. The strength of an absorption for any given absorbing species will be governed by the absorption coefficient, which is nearly 4.5 times stronger at 2.9 μm than at 6.1 μm for liquid water (Wilk et al., 2024). The small amount of H_2O, incorporated externally and/or internally in these samples, may be insufficient to produce a discernable 6 μm feature but sufficient to produce discernible changes in the 3 μm region. We find explanation three to be the most plausible scenario for the data presented here but note that the detection of H_2O in nominally anhydrous minerals will be complicated by the presence of other absorption features in this wavelength region.

4.3.2. Silicate related absorptions

Though there was no H_2O related activity in the 6 μm region for any of the samples in this study, there were notable changes in the spectral slope and strength of non-water related absorptions in the olivine sample following heating. Olivine exhibits a series of fundamental silicate absorptions in the mid-IR region (e.g., Hamilton, 2010; Lane et al., 2011) and has combination-overtone absorptions in the IMIR region, though the associated fundamental absorptions have yet to be identified. We observe no changes in olivine's 5.6 and 6.0 μm silicate features but we do observe changes in spectral slope longward of 6.1 μm for the top, mixed, and bottom sample in addition to a weaker absorption feature at 6.2 μm increasing in strength. The 6.2 μm absorption feature increases in band strength with decreasing strength in the 3 μm hydration feature (Fig. 7), indicating that the observed changes in band strength and spectral slope are due to changing mineralogy, not H_2O related activity. Oxidation of the olivine sample occurred during the heating process and facilitated the formation of hematite, with the most hematite (~1 wt%) in the bottom olivine sample and lesser amounts in the mixed and top olivine sample. The spectral changes are likely attributed to the increasing amounts of hematite in the sample but at present we are

unable to link these changes to the fundamental absorptions in the mid-IR region.

4.4. Implications for lunar remote sensing

Hydrogen bearing volatile species, such as OH and H_2O, can exist on the surface of the lunar regolith or internal to the regolith material. These volatile species may have various origins, including space weathering processes such as solar wind irradiation, the indigenous material during lunar accretion, and cometary or asteroid delivery (e.g., Černok et al., 2020; Greenwood et al., 2011; Lucey et al., 2021; McCord et al., 2011). The source of hydration in our terrestrial samples may differ from that in lunar regolith but studying the effects of internal and external hydration on the reflectance spectra of these lunar relevant minerals can provide insights into what we may expect for the lunar surface.

The lab experiments presented here have applications to ground and space based observations of a 3 μm feature on the lunar surface that is consistent with the presence of OH and/or H_2O (e.g., Clark, 2009; Pieters et al., 2009; Sunshine et al., 2009). Here we observe the effects of a vacuum environment on the strength of the 3 μm feature due to the removal of weakly bound H_2O on olivine and anorthite, though diurnal variations of the 3 μm feature on the Moon will be driven by thermal processes rather than physical removal from the vacuum environment. Both olivine and anorthite have a band minimum position near 2.9 μm and with progressive dehydration an additional absorption feature near 3.1 μm becomes more evident. These absorption features are consistent with both OH and/or H_2O. Initial observations by Deep Impact observed a 3 μm feature whose band minimum was centered at 2.95 μm, which could be consistent with the asymmetric and symmetric modes of H_2O or OH (Sunshine et al., 2009). Sunshine et al., 2009 notes that the presence of the 3.1 μm bending overtone could be diagnostic of H_2O in those observations but because of calibration uncertainties the absorption could not be distinctly resolved. We caution that while the presence of a 3.1 μm absorption feature may be an indicator of H_2O, that OH absorptions may also be produced longward of 3 μm in minerals such as olivine and anorthite due to bound protons on mineral surfaces, potentially from solar wind. While the Moon Mineralogy Mapper (M^3) provides spectral coverage of more than 95 % of the lunar surface, the spectral range (430–3000 nm) of the instrument can detect but not fully resolve the full 3 μm feature (Green et al., 2011). Datasets that resolve the full lunar 3 μm feature (i.e., Lunar Trailblazer, Chandrayaan-2) will be fundamental for our understanding of the lunar water cycle, though special care needs to be taken when interpreting absorption features (OH vs H_2O) in the 3 μm region.

Despite having upwards of 300–400 ppm of water in our most hydrated samples, we are unable to resolve a 6 μm feature associated with the presence or removal of surficial and internal water in both olivine and anorthite. Telescopic observations from SOFIA, however, detect a weak 6 μm emission feature that has been interpreted to be H_2O trapped in impact glasses (Honniball et al., 2021; Reach et al., 2023). An estimated 100–400 ppm of H_2O has been derived from the strength of the 6 μm emission feature in SOFIA data, which is well within the estimated water contents of our samples. Our inability to detect a 6 μm feature in terrestrial analog samples may suggest that the lunar regolith contains a higher abundance of internal water than the samples presented here, implying that either 1) the water content derived from the 3 μm feature in the terrestrial samples is overestimated, or 2) the 6 μm SOFIA observations underestimated water content. It is a possibility that the weak 6 μm emission feature detected by SOFIA may have been erroneously attributed to the presence of water, though it is unclear as to what SOFIA would have otherwise detected. Assuming the lunar 6 μm feature is indeed due to water trapped in impact glasses, understanding how the bonding environment of water affects its detection at this wavelength is crucial and may reconcile why a 6 μm feature is observed in both terrestrial mid-ocean ridge basalt glasses (S. Li and Milliken, 2017) and impact glasses on the lunar surface, yet remains undetected in our terrestrial analog samples with similar water abundances. Ultimately, the detection limits of H_2O at 6 μm merits further laboratory investigations, however, our results indicate that even with derived total water abundances of up to 400 ppm, the 6 μm feature remains undetectable in olivine and anorthite. Given that the SOFIA telescope detects emission rather than reflectance, conducting similar laboratory experiments in emission would yield a more direct comparison to remote sensing observations of the Moon. At present it is unclear as to whether diurnal variations in the strength of the 6 μm feature exist on the lunar surface but our failure to detect surficial H_2O under terrestrial atmospheric conditions, which contains more H_2O than the lunar exosphere, suggests diurnal variations are unlikely.

5. Conclusion

Our study highlights the complexities involved with the detection and interpretation of hydration related features in the 3 and 6 μm regions for lunar relevant nominally anhydrous minerals. Under ambient conditions, our unheated olivine and anorthite samples have derived total water contents of 300–400 ppm and we demonstrate that both external and internal hydration components contribute to the overall shape and strength of the 3 μm hydration feature. We interpret at least a portion of the observed changes to be associated with the removal of H_2O under vacuum conditions or from heating. Our inability to observe the fundamental bending mode of H_2O at 6 μm prevents an unambiguous detection of H_2O and highlights the complications in speciating hydration in nominally anhydrous minerals using 3 and 6 μm observations in the laboratory.

Enhanced resolution reflectance data spanning the entire 3 μm feature will be a welcome addition to existing lunar remote sensing datasets, however we caution that distinguishing between OH and H_2O in this wavelength region may be challenging. Although we were unable to detect a 6 μm H_2O feature in the laboratory, SOFIA observations do reveal a 6 μm H_2O feature. Joint 3 and 6 μm observations of the Moon may still provide valuable insights into the speciation of hydration and continued laboratory and in-situ investigations probing the nature of what is being detected on the lunar surface would be valuable. Understanding the nuanced nature of 3 and 6 μm observations should be of the utmost importance, as the James Webb Space Telescope also covers these wavelengths and could be utilized to detect hydration on bodies throughout our solar system.

CRediT authorship contribution statement

Kierra A. Wilk: Writing – original draft, Investigation, Formal analysis, Data curation, Conceptualization. **J.L. Bishop:** Writing – review & editing, Funding acquisition, Conceptualization. **A. Maturilli:** Resources, Methodology. **C.M. Pieters:** Writing – review & editing. **J.F. Mustard:** Writing – review & editing. **K. Robertson:** Formal analysis, Writing – review & editing.

Declaration of competing interest

The authors declare that they have no known competing financial interests or personal relationships that could have appeared to influence the work reported in this paper.

Acknowledgements

The authors are grateful to the Planetary Spectroscopy Lab at the DLR-Berlin and to G. Alemanno for assistance with the spectral measurements and K. Robertson for assistance with XRD measurements. We are grateful for the support from Europlanet Society grant #22-EPN3-043, LDAP grant # 80NSSC21K1480, and NASA SSERVI LunaSCOPE grant #80NSSC23M0161. Europlanet 2024 RI has received funding

from the European Union's Horizon 2020 research and innovation programme under grant agreement No 871149. We thank the two anonymous reviewers who provided valuable feedback on this manuscript.

Appendix A. Supplementary data

Supplementary data to this article can be found online at https://doi.org/10.1016/j.icarus.2025.116651.

Data availability

The data is publicly available at https://doi.org/10.7910/DVN/LMB0FY

References

Barrett, T.J., Robinson, K.L., Barnes, J.J., Jeffrey Taylor, G., Nagashima, K., Huss, G.R., Franchi, I.A., Anand, M., Kring, D.A., 2023. Deciphering the origin(s) of H and cl in Apollo 15 quartz monzodiorites: evidence for multiple processes and reservoirs. Geochim. Cosmochim. Acta 358, 192–206. https://doi.org/10.1016/j.gca.2023.08.004.

Bishop, J.L., Pieters, C.M., Hiroi, T., Mustard, J.F., 1998. Spectroscopic analysis of Martian meteorite Allan Hills 84001 powder and applications for spectral identification of minerals and other soil components on Mars. Meteorit. Planet. Sci. 33 (4), 699–707. https://doi.org/10.1111/j.1945-5100.1998.tb01676.x.

Bowell, E., Hapke, B., Domingue, D., Lumme, K., Peltoniemi, J., Harris, A., 1998. Application of photometric models to asteroids. In: Asteroids II. University of Arizona Press, pp. 524–556.

Boyce, J.W., Liu, Y., Rossman, G.R., Guan, Y., Eiler, J.M., Stolper, E.M., Taylor, L.A., 2010. Lunar apatite with terrestrial volatile abundances. Nature 466 (7305), 466–469. https://doi.org/10.1038/nature09274.

Černok, A., Anand, M., Zhao, X., Darling, J.R., White, L.F., Stephant, A., Dunlop, J., Tait, K.T., Franchi, I.A., 2020. Preservation of primordial signatures of water in highly-shocked ancient lunar rocks. Earth Planet. Sci. Lett. 544, 116364. https://doi.org/10.1016/j.epsl.2020.116364.

Chauhan, P., Chauhan, M., Verma, P.A., Sharma, S., Bhattacharya, S., Dagar, A.K., Anon, A., Patil, A.N., Parashar, A.K., Kumar, A., Desai, N., Karidhal, R., Kumar, A.S. K., 2021. Unambiguous detection of OH and H_2O on the Moon from Chandrayaan-2 Imaging Infrared Spectrometer reflectance data using 3 μm hydration feature. Curr. Sci. 121 (3), 391. https://doi.org/10.18520/cs/v121/i3/391-401.

Clark, R.N., 2009. Detection of adsorbed water and hydroxyl on the moon. Science 326 (5952), 562–564. https://doi.org/10.1126/science.1178105.

Dyar, M.D., Hibbitts, C.A., Orlando, T.M., 2010. Mechanisms for incorporation of hydrogen in and on terrestrial planetary surfaces. Icarus 208 (1), 425–437. https://doi.org/10.1016/j.icarus.2010.02.014.

Green, R.O., Pieters, C., Mouroulis, P., Eastwood, M., Boardman, J., Glavich, T., Isaacson, P., Annadurai, M., Besse, S., Barr, D., Buratti, B., Cate, D., Chatterjee, A., Clark, R., Cheek, L., Combe, J., Dhingra, D., Essandoh, V., Geier, S., Wilson, D., 2011. The Moon Mineralogy Mapper (M^3) imaging spectrometer for lunar science: Instrument description, calibration, on-orbit measurements, science data calibration and on-orbit validation. J. Geophys. Res. 116, E00G19. https://doi.org/10.1029/2011JE003797.

Greenwood, J.P., Itoh, S., Sakamoto, N., Warren, P., Taylor, L., Yurimoto, H., 2011. Hydrogen isotope ratios in lunar rocks indicate delivery of cometary water to the moon. Nat. Geosci. 4 (2), 79–82. https://doi.org/10.1038/ngeo1050.

Grumpe, A., Wöhler, C., Berezhnoy, A.A., Shevchenko, V.V., 2019. Time-of-day-dependent behavior of surficial lunar hydroxyl/water: observations and modeling. Icarus 321, 486–507. https://doi.org/10.1016/j.icarus.2018.11.025.

Hamilton, V.E., 2010. Thermal infrared (vibrational) spectroscopy of mg–Fe olivines: a review and applications to determining the composition of planetary surfaces. Geochemistry 70 (1), 7–33. https://doi.org/10.1016/j.chemer.2009.12.005.

Hapke, B., 2012. Theory of Reflectance and Emittance Spectroscopy, 2nd ed. Cambridge University Press. https://doi.org/10.1017/CBO9781139025683.

Hauri, E.H., Weinreich, T., Saal, A.E., Rutherford, M.C., Van Orman, J.A., 2011. High pre-eruptive water contents preserved in lunar melt inclusions. Science 333 (6039), 213–215. https://doi.org/10.1126/science.1204626.

Hendrix, A.R., Hurley, D.M., Farrell, W.M., Greenhagen, B.T., Hayne, P.O., Retherford, K. D., Vilas, F., Cahill, J.T.S., Poston, M.J., Liu, Y., 2019. Diurnally migrating lunar water: evidence from ultraviolet data. Geophys. Res. Lett. 46 (5), 2417–2424. https://doi.org/10.1029/2018GL081821.

Hibbitts, C.A., Grieves, G.A., Poston, M.J., Dyar, M.D., Alexandrov, A.B., Johnson, M.A., Orlando, T.M., 2011. Thermal stability of water and hydroxyl on the surface of the moon from temperature-programmed desorption measurements of lunar analog materials. Icarus 213 (1), 64–72. https://doi.org/10.1016/j.icarus.2011.02.015.

Honniball, C.I., Lucey, P.G., Ferrari-Wong, C.M., Flom, A., Li, S., Kaluna, H.M., Takir, D., 2020. Telescopic observations of lunar hydration: variations and abundance. J. Geophys. Res.: Planet. 125 (9), e2020JE006484. https://doi.org/10.1029/2020JE006484.

Honniball, C.I., Lucey, P.G., Li, S., Shenoy, S., Orlando, T.M., Hibbitts, C.A., Hurley, D. M., Farrell, W.M., 2021. Molecular water detected on the sunlit moon by SOFIA. Nature Astronom. 5 (2), 121–127. https://doi.org/10.1038/s41550-020-01222-x.

Honniball, C.I., Lucey, P.G., Arredondo, A., Reach, W.T., Malaret, E.R., 2022. Regional map of molecular water at high southern latitudes on the moon using 6 μm data from the stratospheric Observatory for Infrared Astronomy. Geophys. Res. Lett. 49 (9). https://doi.org/10.1029/2022GL097786.

Hu, S., He, H., Ji, J., Lin, Y., Hui, H., Anand, M., Tartèse, R., Yan, Y., Hao, J., Li, R., Gu, L., Guo, Q., He, H., Ouyang, Z., 2021. A dry lunar mantle reservoir for young mare basalts of Chang'e-5. Nature 600 (7887), 49–53. https://doi.org/10.1038/s41586-021-04107-9.

Johnson, E.A., Rossman, G.R., 2004. A survey of hydrous species and concentrations in igneous feldspars. Am. Mineral. 89 (4), 586–600. https://doi.org/10.2138/am-2004-0413.

Kremer, C.H., Mustard, J.F., Pieters, C.M., 2020. Cross-over infrared spectroscopy: a new tool for the remote determination of olivine composition. Geophys. Res. Lett. 47 (20). https://doi.org/10.1029/2020GL089151.

Laferriere, K.L., Sunshine, J.M., Feaga, L.M., 2022. Variability of hydration across the southern hemisphere of the moon as observed by deep impact. J. Geophys. Res.: Planet. 127 (8). https://doi.org/10.1029/2022JE007361.

Lane, M.D., Bishop, J.L., 2019. In: Bishop, J.L., Moersch, J.E., Bell III, J.F. (Eds.), Chapter 3: Mid-infrared (thermal) emission and reflectance spectroscopy, Remote Compositional analysis: Techniques for Understanding spectroscopy, Mineralogy, and Geochemistry of Planetary Surfaces, 1st ed. Cambridge University Press. https://doi.org/10.1017/9781316888872.

Lane, M.D., Glotch, T.D., Dyar, M.D., Pieters, C.M., Klima, R., Hiroi, T., Bishop, J.L., Sunshine, J., 2011. Midinfrared spectroscopy of synthetic olivines: thermal emission, specular and diffuse reflectance, and attenuated total reflectance studies of forsterite to fayalite. J. Geophys. Res. 116 (E8), E08010. https://doi.org/10.1029/2010JE003588.

Le Losq, C., Jollands, M.C., Tollan, P.M.E., Hawkins, R., O'Neill, H.St., C., 2019. Point defect populations of forsterite revealed by two-stage metastable hydroxylation experiments. Contrib. Mineral. Petrol. 174 (6), 53. https://doi.org/10.1007/s00410-019-1590-6.

Li, S., Li, L., 2011. Radiative transfer modeling for quantifying lunar surface minerals, particle size, and submicroscopic metallic Fe. J. Geophys. Res.: Planet. 116 (E9). https://doi.org/10.1029/2011JE003837, 2011JE003837.

Li, S., Milliken, R.E., 2017. Water on the surface of the moon as seen by the moon mineralogy mapper: distribution, abundance, and origins. Sci. Adv. 3 (9), e1701471. https://doi.org/10.1126/sciadv.1701471.

Li, Y., Will Mackwell, S.J., Kohlstedt, D.L., 2022. Diffusion rates of hydrogen defect species associated with site-specific infrared spectral bands in natural olivine. Earth Planet. Sci. Lett. 581, 117406. https://doi.org/10.1016/j.epsl.2022.117406.

Libowitzky, E., 2006. The structure of hydrous species in nominally anhydrous minerals: information from polarized IR spectroscopy. Rev. Mineral. Geochem. 62 (1), 29–52. https://doi.org/10.2138/rmg.2006.62.2.

Livengood, T.A., Chin, G., Sagdeev, R.Z., Mitrofanov, I.G., Boynton, W.V., Evans, L.G., Litvak, M.L., McClanahan, T.P., Sanin, A.B., Starr, R.D., Su, J.J., 2015. Moonshine: diurnally varying hydration through natural distillation on the moon, detected by the lunar exploration neutron detector (LEND). Icarus 255, 100–115. https://doi.org/10.1016/j.icarus.2015.04.004.

Lucey, P.G., Petro, N., Hurley, D.M., Farrell, W.M., Prem, P., Costello, E.S., Cable, M.L., Barker, M.K., Benna, M., Dyar, M.D., Fisher, E.A., Green, R.O., Hayne, P.O., Hibbitts, K., Honniball, C., Li, S., Malaret, E., Mandt, K., Mazarico, E., Orlando, T., 2021. Volatile interactions with the lunar surface. Geochemistry, 125858. https://doi.org/10.1016/j.chemer.2021.125858.

McCord, T.B., Taylor, L.A., Combe, J.-P., Kramer, G., Pieters, C.M., Sunshine, J.M., Clark, R.N., 2011. Sources and physical processes responsible for OH/H_2O in the lunar soil as revealed by the Moon Mineralogy Mapper (M^3). J. Geophys. Res. 116, E00G05. https://doi.org/10.1029/2010JE003711.

Milliken, R.E., Li, S., 2017. Remote detection of widespread indigenous water in lunar pyroclastic deposits. Nat. Geosci. 10 (8), 561–565. https://doi.org/10.1038/ngeo2993.

Milliken, R.E., Mustard, J.F., 2005. Quantifying absolute water content of minerals using near-infrared reflectance spectroscopy. J. Geophys. Res. 110 (E12), E12001. https://doi.org/10.1029/2005JE002534.

Mustard, J.F., Pieters, C.M., 1989. Photometric phase functions of common geologic minerals and applications to quantitative analysis of mineral mixture reflectance spectra. J. Geophys. Res. Solid Earth 94 (B10), 13619–13634. https://doi.org/10.1029/JB094iB10p13619.

Nyquist, R.A., Putzig, C.L., Leugers, M.A., Kagel, R.O., Nyquist, R.A., 1997. The Handbook of Infrared and Raman Spectra of Inorganic Compounds and Organic Salts. Academic Press.

Pieters, C.M., Goswami, J.N., Clark, R.N., Annadurai, M., Boardman, J., Buratti, B., Combe, J.-P., Dyar, M.D., Green, R., Head, J.W., Hibbitts, C., Hicks, M., Isaacson, P., Klima, R., Kramer, G., Kumar, S., Livo, E., Lundeen, S., Malaret, E., Varanasi, P., 2009. Character and spatial distribution of OH/H_2O on the surface of the moon seen by M^3 on Chandrayaan-1. Science 326 (5952), 568–572. https://doi.org/10.1126/science.1178658.

Reach, W.T., Lucey, P.G., Honniball, C.I., Arredondo, A., Malaret, E.R., 2023. The distribution of molecular water in the lunar south polar region based upon 6 μm spectroscopic imaging. Planet. Sci. J. 4 (3), 45. https://doi.org/10.3847/PSJ/acbdf2.

Saal, A.E., Hauri, E.H., Cascio, M.L., Van Orman, J.A., Rutherford, M.C., Cooper, R.F., 2008. Volatile content of lunar volcanic glasses and the presence of water in the

moon's interior. Nature 454 (7201), 192–195. https://doi.org/10.1038/nature07047.

Saal, A.E., Hauri, E.H., Van Orman, J.A., Rutherford, M.J., 2013. Hydrogen isotopes in lunar volcanic glasses and melt inclusions reveal a carbonaceous chondrite heritage. Science 340 (6138), 1317–1320. https://doi.org/10.1126/science.1235142.

Salisbury, J.W., Walter, L.S., Vergo, N., 1987. Mid-infrared (2.1—2.5 um) spectra of minerals (open-file report) [open-file report]. U.S. Geological Survey. https://doi.org/10.3133/ofr87263.

Stephant, A., Anand, M., Tartèse, R., Zhao, X., Degli-Alessandrini, G., Franchi, I.A., 2020. The hydrogen isotopic composition of lunar melt inclusions: an interplay of complex magmatic and secondary processes. Geochim. Cosmochim. Acta 284, 196–221. https://doi.org/10.1016/j.gca.2020.06.017.

Sunshine, J.M., Farnham, T.L., Feaga, L.M., Groussin, O., Merlin, F., Milliken, R.E., A'Hearn, M.F., 2009. Temporal and spatial variability of lunar hydration as observed by the deep impact spacecraft. Science 326 (5952), 565–568. https://doi.org/10.1126/science.1179788.

Wilk, K.A., Mustard, J.F., Milliken, R.E., Pieters, C.M., 2024. Variations in surface adsorbed H2O on lunar soils and relevant minerals. Icarus 115945. https://doi.org/10.1016/j.icarus.2024.115945.

Wöhler, C., Grumpe, A., Berezhnoy, A.A., Shevchenko, V.V., 2017. Time-of-day–dependent global distribution of lunar surficial water/hydroxyl. Sci. Adv. 3 (9), e1701286. https://doi.org/10.1126/sciadv.1701286.

Wohlfarth, K., Wöhler, C., Hiesinger, H., Helbert, J., 2023. An advanced thermal roughness model for airless planetary bodies: implications for global variations of lunar hydration and mineralogical mapping of mercury with the MERTIS spectrometer. Astron. Astrophys. 674, A69. https://doi.org/10.1051/0004-6361/202245343.